iJRASET
International Journal For Research in Applied Science and Engineering Technology



INTERNATIONAL JOURNAL FOR RESEARCH

IN APPLIED SCIENCE & ENGINEERING TECHNOLOGY

Volume: 14 **Issue:** V **Month of publication:** May 2026

DOI: https://doi.org/10.22214/ijraset.2026.82126

www.ijraset.com

Call: 08813907089 | E-mail ID: ijraset@gmail.com

International Journal for Research in Applied Science & Engineering Technology (IJRASET)
ISSN: 2321-9653; IC Value: 45.98; SJ Impact Factor: 7.538
Volume 14 Issue V May 2026- Available at www.ijraset.com

Vibration Monitoring in Underground Pipeline Systems Using Fiber Bragg Grating Sensors

Prof. Santosh Jagtap, Akansha Tandale, Ayush Babar, Ayush Thakur, Varsha Venkataraman
Department of Electronics and Telecommunication Engineering Vidyalankar Institute of Technology, Mumbai – 400037, India
University of Mumbai, 2025–26

Abstract*—Underground pipelines are vital to urban society, but are susceptible to vibration, strain from soil displacement, corrosion and temperature fluctuations. Electrical sensors face several challenges, including sensitivity to electromagnetic interference (EMI), lack of distributed sensing capability and stability in the underground environment. We demonstrate a Fiber Bragg Grating (FBG) based structural health monitoring (SHM) system in underground pipelines to monitor vibration.The system integrates three simulation software packages: COMSOL Multiphysics (finite-element modelling of structures), OptiSystem (optical sensor modelling) and MATLAB (frequency-domain signal processing). The strain for FBG sensor design is calculated from COMSOL's Von Mises stress. OptiSystem modelling is used to evaluate the Bragg wavelength shift with strain (01500 με) and temperature (0-180 °C). The MATLAB Fast Fourier Transform (FFT) is utilised to analyse vibration with combined FBG sensors. The system has strain sensitivity of 1.0-1.2 pm/με, temperature sensitivity of 14.3 pm/°C, grating length of 10-15 mm and vibration frequency of 10 Hz. This approach provides a scalable, EMI-proof and sensitive system for smart cities, smart maintenance and real-time fault detection in oil and gas, metro and utility pipelines.

Index Terms*—Fiber Bragg Grating, Structural Health Monitoring, Underground Pipelines, Vibration Analysis, COMSOL Multiphysics, OptiSystem, Fast Fourier Transform, Wavelength Shift, Strain Sensing, Corrosion Monitoring.

I. INTRODUCTION

The increase of the underground infrastructure, such as petroleum and gas pipes, water and sewer pipes, metro tunnels and conduits have created a dire reliance on the underground structure. They are exposed to a multifaceted dynamic loading, which includes traffic vibration, earthquake, differential soil settlements, hydrostatic soil pressure and thermal expansion. Such type of loading leads to deterioration (fatigue cracks, corrosion growth, wall thinning and settlements). These damages cannot be detected until the catastrophic failure, unless they are in constant monitoring.

The need of the problem is demonstrated by accidents. Patterns of unnoticed defects of underground pipeline systems are mentioned in industrial reports such as gas leaks of the pressure systems leading to emergency shutdowns are reported [6], [7]. These events demonstrate the need for timeconsuming manual inspections and the need for continuous, real-time, distributed, SHM systems.

Conventional monitoring uses electrical transducers - piezoelectric accelerometers, resistive strain gauges and capacitive pressure sensors. These have strong shortcomings in underground applications: they are vulnerable to EMI on nearby power systems, prone to electrochemical corrosion in wet soils, and signal attenuation during long-range transmission, and are point-localised in measurement, limiting distributed structural characterisation.

Fiber Bragg Grating (FBG) sensors have been proposed as an attractive substitute to SHM in harsh environments, and they take advantage of the periodic refractive index modulation written into a single-mode optical fiber to reflect a given Bragg wavelength that is sensitive to external disturbances. The fundamental Bragg condition is:

$$\lambda_B = 2n_{\text{eff}}\Lambda \qquad (1)$$

where λ_B is the Bragg wavelength, n_{eff} is the effective refractive index, and Λ is the grating period. Any perturbation modifying n_{eff} or Λ—from axial strain or temperature— produces a measurable wavelength shift.

This paper suggests a combined FBG-based SHM system using COMSOL Multiphysics, OptiSystem and MATLAB as a part of the single approach to underground pipeline vibration monitoring.

II. LITERATURE REVIEW

FBG sensors have been extensively researched for civil, geotechnical, and industrial structural health monitoring (SHM). Bhaskar *et al.* [1] established the theoretical foundation for FBG dual-parameter sensitivity characterization. Tripathy [2] validated OptiSystem for FBG strain simulation and demonstrated a linear relationship between wavelength shift and applied strain. More *et al.*

©IJRASET: All Rights are Reserved

[3] confirmed the robustness of FBG sensors at 1550 nm for long-distance monitoring. Qiao *et al.* [4] demonstrated multi-parameter FBG sensing, including vibration, acoustic waves, pressure, and temperature, in oil and gas pipeline environments. Razi *et al.* [5] verified the linear proportionality between strain and wavelength shift in OptiSystem simulations. Chalgham *et al.* [8] developed a coupled electrochemical–mechanical COMSOL model to analyze corrosion in buried pipelines.

The literature review supports high-sensitivity multiparameter measurements with FBG sensors, validation of the simulation platform OptiSystem, stress-corrosion multiparameter modeling with COMSOL, and frequency-domain extraction of vibrations. The current study adds to the new integrated scheme incorporating all three realms.

III. PROBLEM STATEMENT

Buried pipeline networks are critical assets whose inability to sustain the structure leads to safety, environmental and financial consequences. The structure can operate in a complex mechanical and electrochemically hostile environment subject to axial and hoop stresses, dynamic vibration and material degradation from corrosion. Current electrical sensor systems are inherently unsuitable for underground applications: EMI susceptibility, corrosive soil for sensor longevity and limited sensor coverage (point measurement) that prevents accurate distributed structural assessment. This calls for a better sensing technology that can: (i) measure strain and vibration in realtime; (ii) is EMI immune; (iii) holds up over time under corrosive conditions and (iv) links structural analysis, optical sensing and signal processing into a single analytical framework.

IV. PROPOSED METHODOLOGY

A. FBG Sensing Principles

For strain sensing, axial strain ε changes n_{eff} due to the photoelastic effect and changes Λ due to the stretching of the fiber:

$$\Delta\lambda_B = \lambda_B(1 - p_e)\varepsilon \quad (2)$$

with $p_e \approx 0.22$ being the photoelastic constant of silica fiber, resulting in a theoretical sensitivity of $\approx 1.2\text{pm}/\mu\varepsilon$ at 1550nm.

The thermal sensitivity is due to the thermal expansion and the thermo-optic effect:

$$\Delta\lambda_B = \lambda_B(\alpha + \xi)\Delta T \quad (3)$$

where $\alpha \approx 0.55 \times 10^{-6}/^{\circ}\text{C}$ and $\xi \approx 8.6 \times 10^{-6}/^{\circ}\text{C}$. Both processes are present in the underground environment:

$$\Delta\lambda_B = \lambda_B\left[(1 - p_e)\,\varepsilon + (\alpha + \xi)\,\Delta T\right] \quad (4)$$

When measuring vibration, dynamic strain is represented by:

$$\varepsilon(t) = \varepsilon_0 \sin(\omega t) \quad (5)$$

The dynamic Bragg wavelength shift contains vibration information obtained using FFT.

B. Integrated Multi-Tool Workflow

Our proposed SHM system is based on a five-stage process.

Stage 1 - Structural Modeling (COMSOL): 3D FEM model of the buried pipeline with soil-pipeline interaction and corrosion defect geometry is built. Governing equation:

$$[K]\{u\} = \{F\} \quad (6)$$

Von Mises stress:

$$\sigma_v = \sqrt{\tfrac{1}{2}\left[(\sigma_1-\sigma_2)^2+(\sigma_2-\sigma_3)^2+(\sigma_3-\sigma_1)^2\right]} \quad (7)$$

Stage 2 — Stress-to-Strain Conversion:

$$\varepsilon = \sigma/E \quad (8)$$

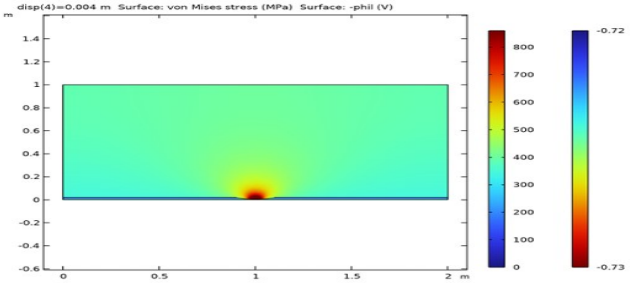


Fig. 1. Von Mises stress distribution in pipeline and electrolyte potential in the soil domain at 4mm prescribed displacement. Peak stress exceeds 800MPa at the corrosion defect center.

Stage 3 — Optical Sensing (OptiSystem): Strain information is applied to simulated FBG sensors; wavelength shifts are calculated.
Stage 4 — FBG Optimization: Grating length (0.8-24mm) and Δn are varied to improve reflectivity, SNR and resolution.
Stage 5 — Vibration Signal Processing (MATLAB):
Trend removal, high-pass filtering, FFT:

$$Y(f) = \sum_{n=0}^{N-1} y(n) e^{-j2\pi fn/N} \quad (9)$$

V. SYSTEM DESIGN AND IMPLEMENTATION

A. FBG Sensor Specification

The T99 high-strength single-mode FBG sensor [12] supports wavelengths 980–1622nm, reflectivities 1–99%, strain range >30,000$\mu\varepsilon$, and temperature range −40°C to +100°C.

B. COMSOL Structural and Corrosion Analysis

Fig. 1 shows the von Mises stress distribution and electrolyte potential at 4mm displacement. Stress peaks at ≈ 800MPa at the corrosion defect center, while the electrolyte potential shows localized anodic activity, confirming stress-corrosion coupling.
Figs. 2 and 3 show stress and corrosion potential variation along the defect for 1–4mm displacements. Stress peaks increase systematically with displacement; corrosion potential becomes more negative, confirming accelerated electrochemical degradation under mechanical load.
Fig. 4 shows corrosion defect evolution at t = 0 and t = 20years. Defect depth approximately doubles with most severe degradation at the center.
Figs. 5 and 6 compare stress and corrosion potential at t = 0 versus t = 20years, demonstrating a ≈ 45% increase in stress concentration at the defect center.

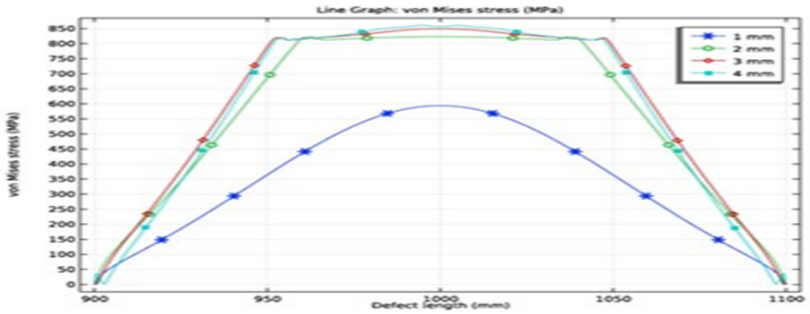


Fig. 2. Von Mises stress along corrosion defect length for prescribed displacements of 1, 2, 3, and 4mm.

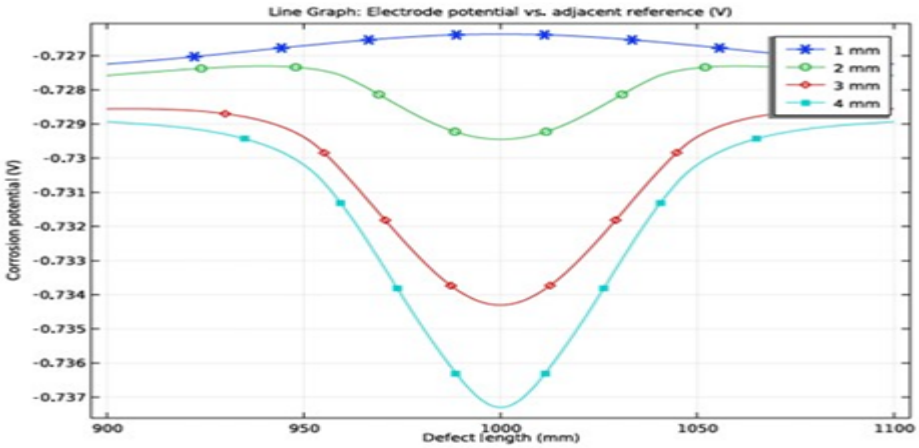


Fig. 3. Corrosion potential distribution along the defect length for 1–4mm displacement. More negative potentials confirm accelerated anodic activity.

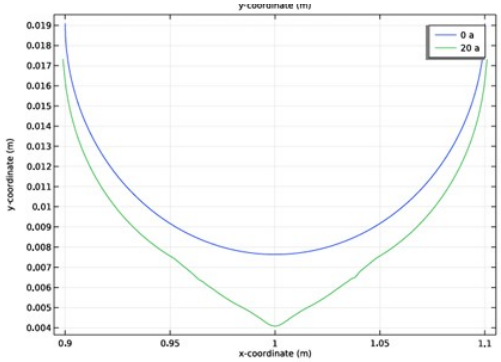


Fig. 4. Corrosion defect profile evolution at t =0 and t =20years showing progressive deepening at the defect center due to stress-corrosion coupling.

C. FBG Grating Length Optimization

Figs. 7–13 show reflection spectra and OSA outputs for key grating lengths, illustrating the evolution from under-coupled short gratings to the optimal 15mm design.

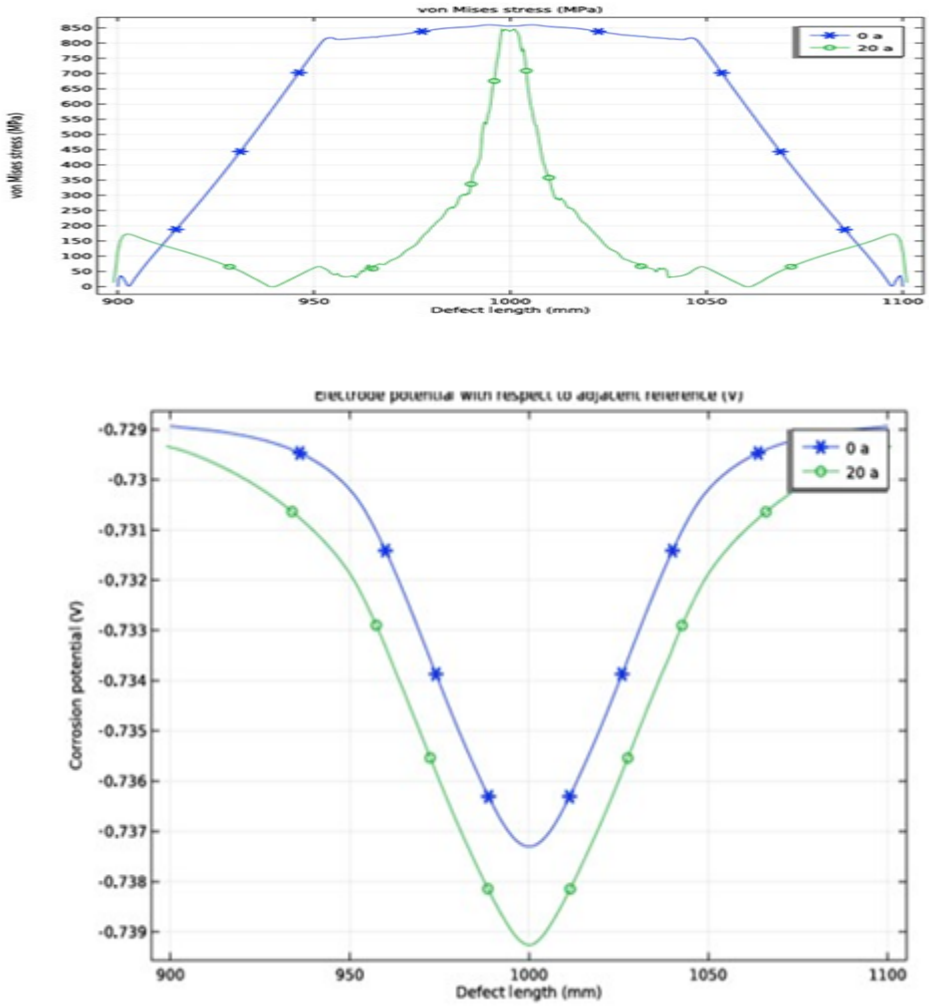


Fig. 5. Von Mises stress along corrosion defect at t =0 and t =20years. Progressive stress concentration reflects material loss and structural weakening.

©IJRASET: All Rights are Reserved

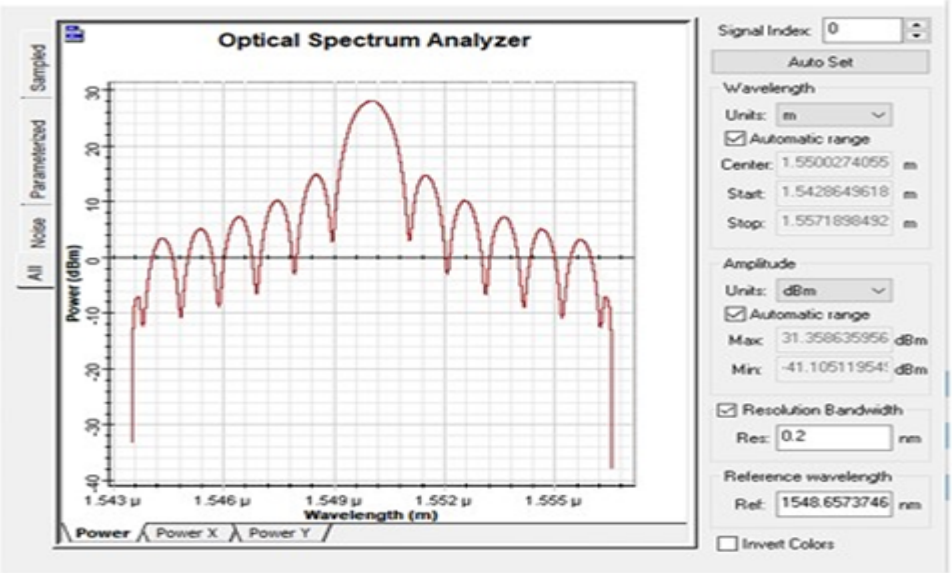


Fig. 6. Corrosion potential at t = 0 and t = 20years showing increased anodic activity at the defect center over the service life.

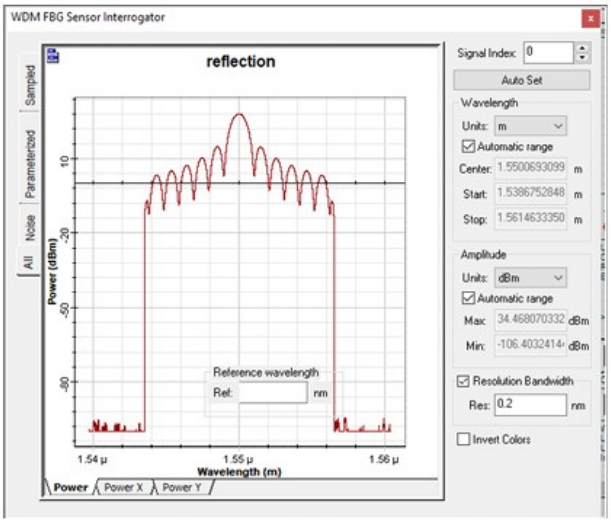


Fig. 7. Reflection spectrum at 0.8mm grating length showing multi-lobed, low-reflectivity response of under-coupled short gratings.

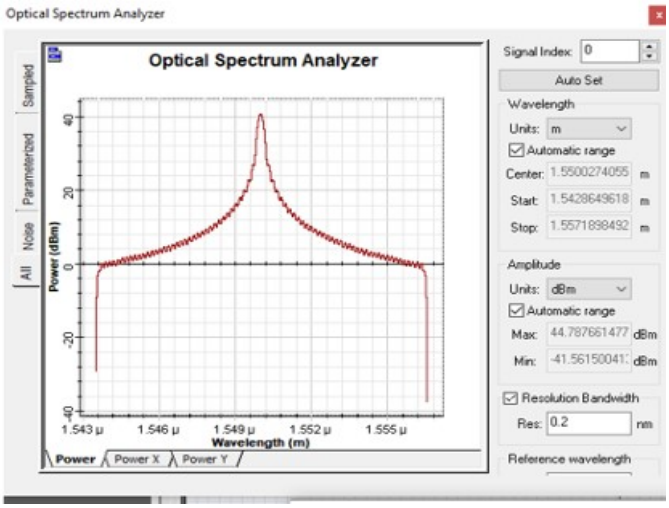


Fig. 8. OSA output at 0.8mm grating length. Broad spectral response confirms insufficient grating coupling.

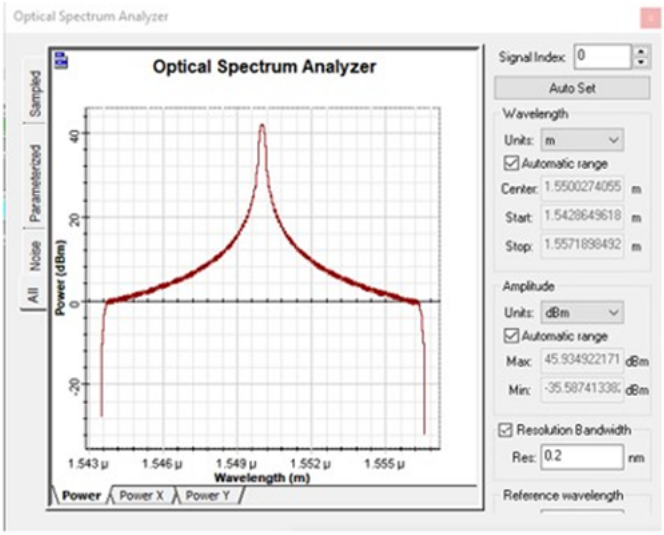


Fig. 9. OSA output at 5mm grating length. Peak power =−4.55dBm with improved but sub-optimal spectral purity (reflectivity 35%).

TABLE I
FBG GRATING LENGTH PERFORMANCE COMPARISON

L(mm)	Pk(dBm)	Refl	SNR	κL	FWHM	Δn
5	−4.55	35%	95.5	0.68	105pm	6.7×10^{-5}
10	−2.90	51%	97.1	0.90	52pm	4.4×10^{-5}
15	**−1.60**	69%	98.4	1.19	35pm	$\mathbf{3.9\times10^{-5}}$
20	−7.30	19%	92.7	0.47	26pm	1.2×10^{-5}
24	−93.95	≈0	6.0	≈0	22pm	4×10^{-10}

= Optimal selection

D. Refractive Index Modulation

Fig. 14 shows the OSA output for Δn = 0.0001. Low modulation produces excessive spectral side lobes and low SLSR ≈ 16dB. Optimal modulation $\Delta n \approx 10^{-4}$ provides the

Fig. 10. OSA output at 10mm grating length. Peak power =−2.9dBm with a well-defined Bragg peak, confirming strong grating coupling (reflectivity 51%).

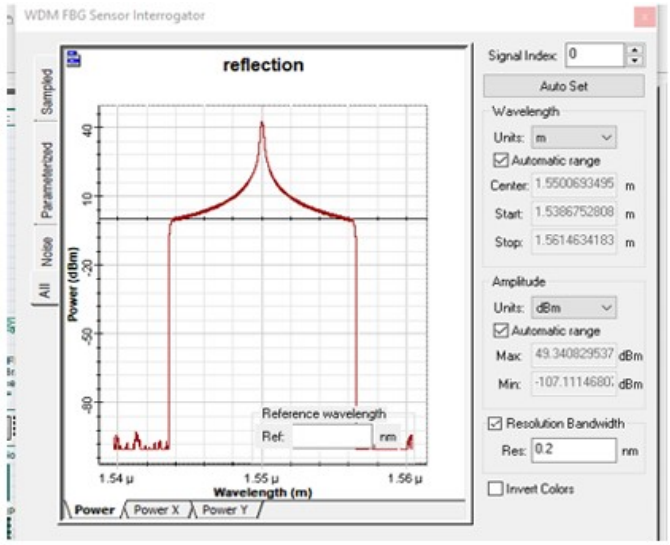
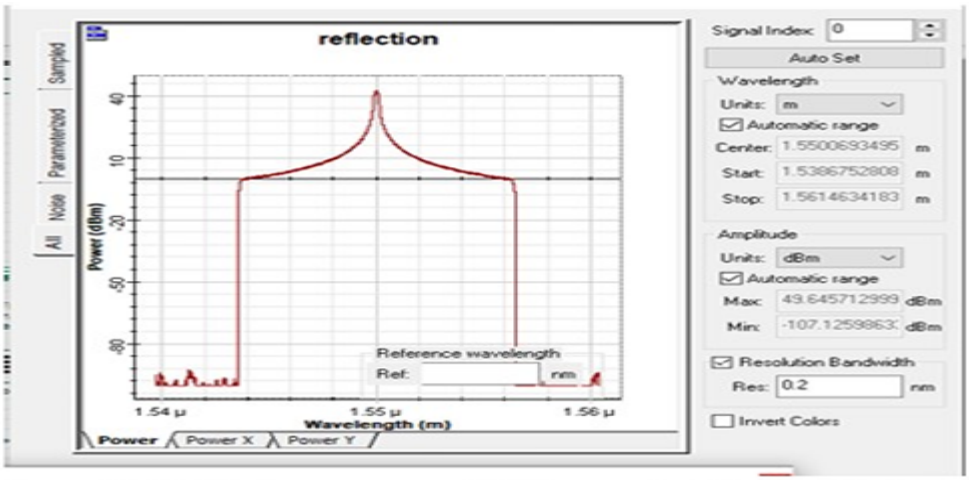


Fig. 11. WDM reflection spectrum at 10mm grating length showing high peak power and good spectral purity.



best balance of reflection strength and spectral purity. Final optimized parameters: grating length 10–15mm, $\Delta n \approx 10^{-4}$, reflectivity 60–70%, SLSR ≈ 16dB.

E. Strain Sensing System

Fig. 15 shows the OptiSystem model for FBG strain sensing, comprising a white light source (193.1THz), bidirectional optical fiber (0.002km), two FBG sensors at 1550nm and 1552nm with temperature compensation, WDM interrogator, and OSA.

Fig. 16 shows the baseline OSA output at zero strain, confirming a well-defined Bragg peak at 1550nm with SNR = 33.72dB.

Fig. 12. Reflection spectrum at 15mm grating length achieving peak reflectivity of 69%, OSA power =−1.6dBm.

Fig. 13. OSA output at 15mm grating length: maximum reflectivity (69%), narrowest FWHM (35pm), and highest SNR (98.4dB). Identified as optimal design.

TABLE II
FBG STRAIN SENSING PERFORMANCE ($T^{=25°}$C)

Strain ($\mu\varepsilon$)	λ (nm)	$\Delta\lambda$ (nm)	S (pm/$\mu\varepsilon$)	SNR (dB)
0	1550.00	0.00	—	+33.72
200	1550.20	0.20	1.0	−15.69
500	1550.50	0.50	1.0	−52.99
1000	1550.75	0.75	1.2	−19.14
1500	1556.40	6.40	4.2	−42.70

Table II summarizes strain sensing performance across 0– 1500$\mu\varepsilon$.

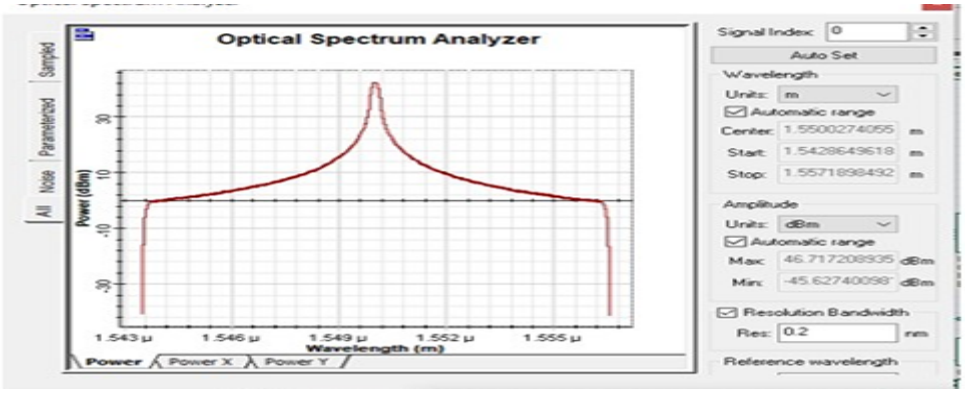


Fig. 14. OSA output for Δn =0.0001 showing broad spectral response with significant side lobes. Optimal $\Delta n \approx 10^{-4}$ balances reflection and spectral purity.

Fig. 17 shows the OptiSystem temperature sensing model with a CW laser and 10mm FBG sensor swept from 0 to 180°C.

Figs. 18 and 19 show the initial Bragg peak at 0°C and the significantly red-shifted peak at 180°C, confirming consistent 14.3pm/°C sensitivity.

Table III confirms constant sensitivity, FWHM, and SNR across 0–180°C.

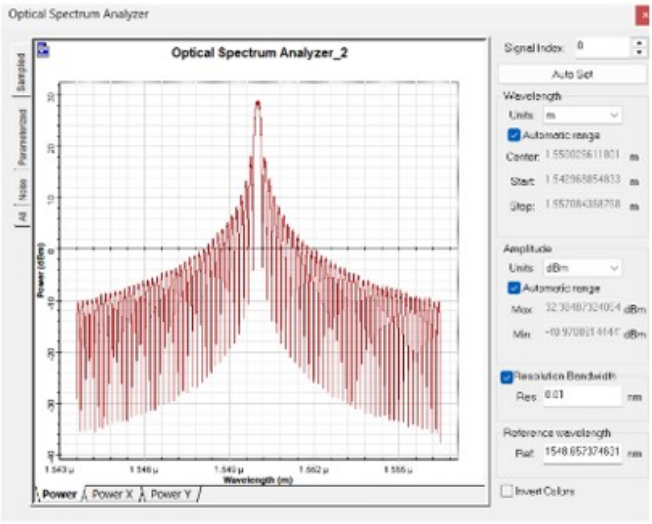
G. 2D Electromagnetic and 3D FBG Models

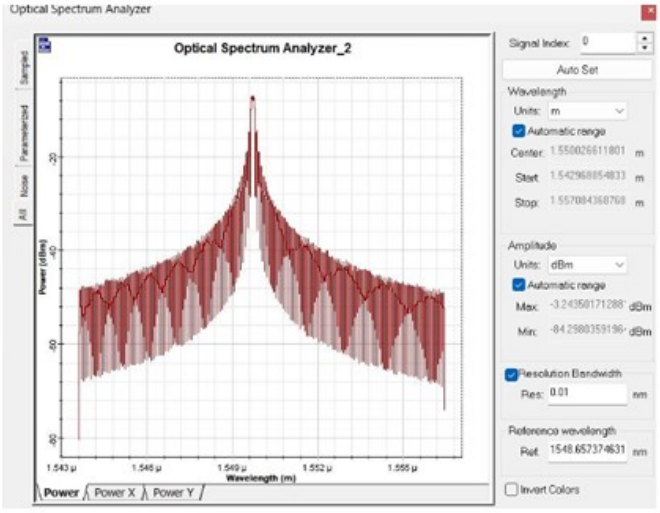
Fig. 20 shows the 2D COMSOL electromagnetic simulation at 193.41THz. Electric field is strongly confined in the fiber core with periodic grating modulation confirming Bragg reflection. Computed effective mode index $n_{eff} \approx 1.5$.

Fig. 21 presents the reflectance, transmittance, and absorbance spectrum confirming a sharp reflectance peak near 1550nm.

Fig. 16. OSA output at 0$\mu\varepsilon$ showing the initial Bragg peak at 1550nm with baseline SNR =33.72dB.

TABLE III





TEMPERATURE ANALYSIS OF FBG SENSOR (STRAIN =0)

T(°C)	S	FWHM	SNR	*R*2	DL(°C)
0	14.3	0.25	91	0.99	0.7
20	14.3	0.25	91	0.99	0.7
40	14.3	0.25	91	0.99	0.7
60	14.3	0.25	91	0.99	0.7
80	14.3	0.25	91	0.99	0.7
100	14.3	0.25	91	0.99	0.7
180	14.3	0.25	91	0.99	0.7

S = pm/°C, DL = Detection Limit

Fig. 22 shows the 3D COMSOL FBG geometry: fiber core (r = 9μm, n_1 = 1.4457), cladding (r = 50μm, n_2 = 1.4378), grating region (n_3 = 1.446, Λ = 454.3nm, N = 100 periods), and photoelastic coefficient p_e = 0.22.

Fig. 18. OSA output at 0°C showing the reference Bragg peak at 1550nm. SNR = 91dB and FWHM = 0.25nm remain constant across all temperatures.

©IJRASET: All Rights are Reserved

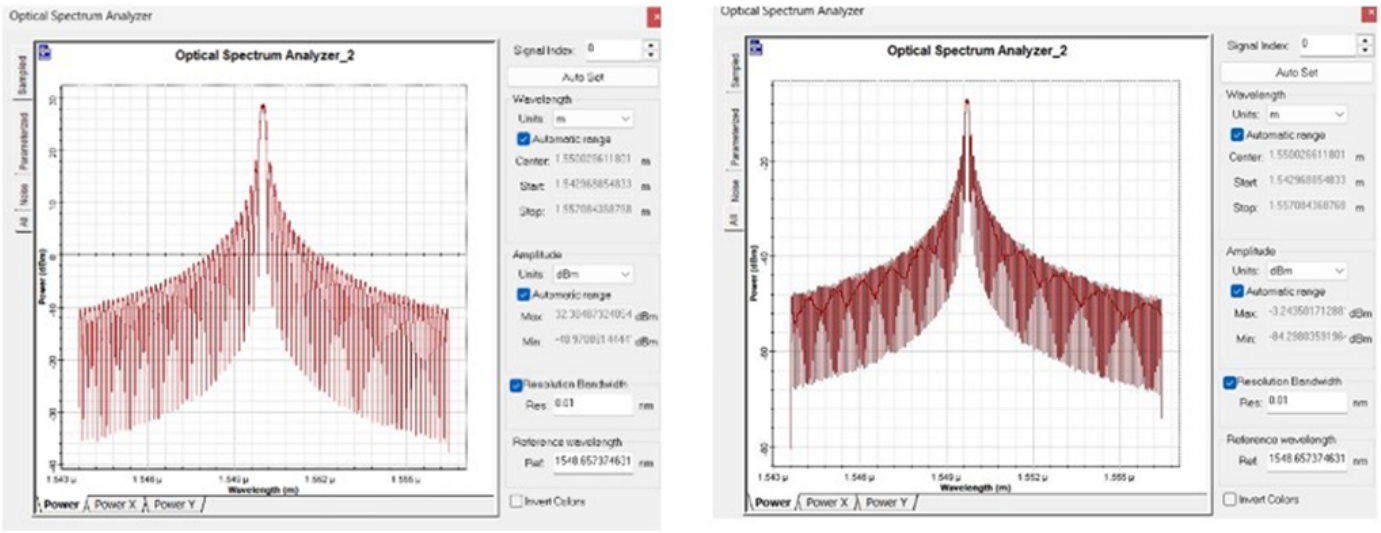
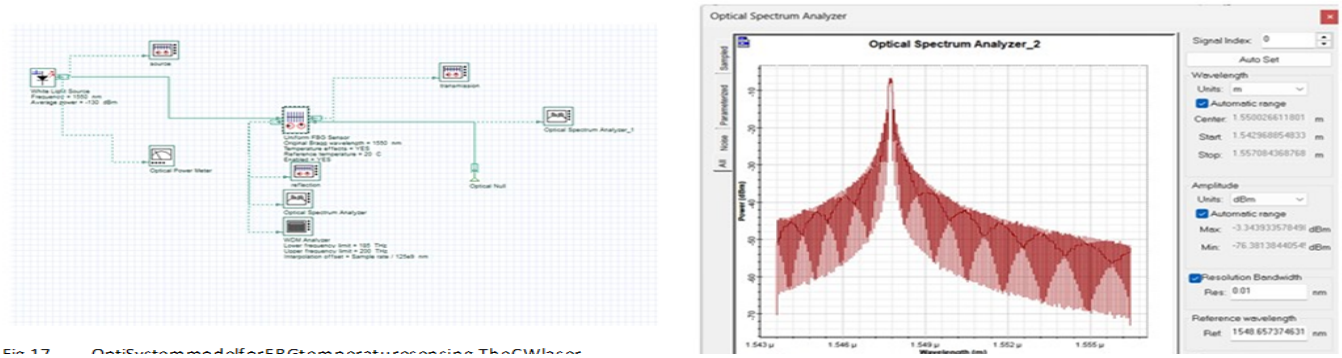


Fig. 19. OSA output at 180˚C showing significant red-shift in the Bragg peak, confirming consistent temperature sensitivity of 14.3pm/˚C.



VI. RESULTS AND DISCUSSION

A. Structural Analysis and Corrosion Coupling

COMSOL simulations reveal strong coupling between mechanical stress and electrochemical corrosion. At 4mm displacement, von Mises stress exceeds 800MPa at the defect center—above the elastic limit of pipeline steels (250– 450MPa)—indicating active plastic deformation. Corrosion potential simultaneously drops to ≈ −0.738V, confirming preferential anodic dissolution at the stressed region. Over 20 years, stress concentration increases by ≈ 45% and defect depth approximately doubles, providing a continuously growing strain signature for FBG monitoring.

B. Grating Optimization and Optical Performance

The optimization study identifies critical grating strength $\kappa L \approx 1.0–1.2$ for maximum reflectivity, corresponding to

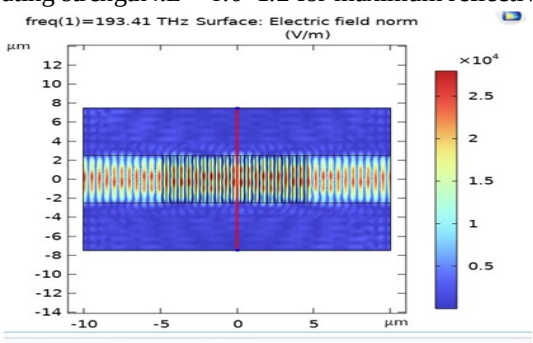


Fig. 20. 2D FBG electric field norm at 193.41THz. Strong field confinement in the fiber core with periodic grating modulation confirms Bragg reflection physics. Effective mode index $n_{eff} \approx 1.5$.

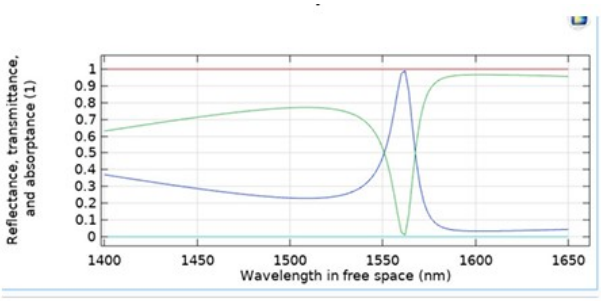


Fig. 21. Reflectance, transmittance, and absorbance spectrum of the FBG as a function of wavelength. A sharp reflectance peak near 1550nm is accompanied by a complementary transmittance dip.

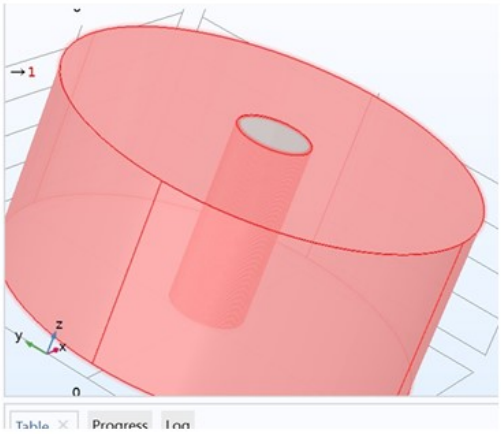


Fig. 22. 3D COMSOL geometry of the FBG model showing the cylindrical fiber core (inner, 9μm radius) and cladding (outer, 50μm radius). The grating region occupies the core along the longitudinal axis.

10–15mm. The 15mm design achieves peak reflectivity 69%, SNR 98.4dB, and FWHM 35pm. Refractive index modulation $\Delta n \approx 10^{-4}$ provides the optimal balance of reflection strength and spectral purity (SLSR ≈ 16dB).

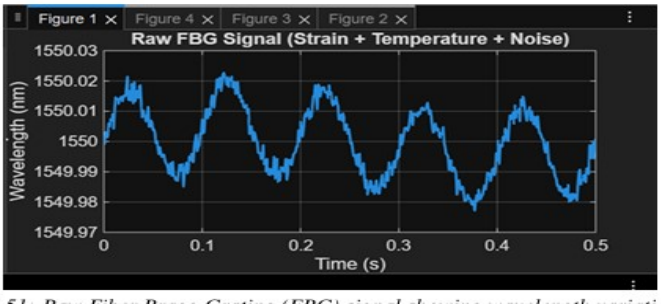


Fig. 23. Raw FBG signal showing combined effects of dynamic strain, temperature drift, and noise over a 0.5s window. Low-frequency thermal drift is clearly visible superimposed on the vibration oscillations.

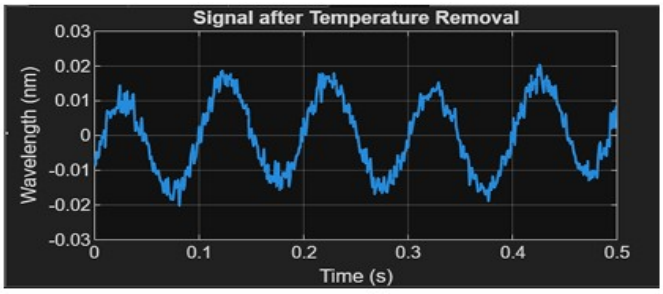


Fig. 24. FBG signal after polynomial detrending for temperature drift removal. The zero-mean oscillatory signal reveals the underlying vibrationinduced component.

C. Vibration Signal Processing

Fig. 23 shows the raw FBG signal with oscillatory behavior and superimposed low-frequency thermal drift (≈ ±0.03nm amplitude). After detrending (Fig. 24), the thermal component is eliminated. High-pass filtering (Fig. 25) isolates clean periodic vibration oscillations of amplitude ≈±0.025nm. FFT analysis (Fig. 26) identifies the dominant vibration frequency at:

$$f_{\text{vibration}} = 9.98\text{Hz} \approx 10\text{Hz} \quad (10)$$

This is consistent with vibration signatures from underground pipeline loading due to surface traffic and low-frequency ground motion.

D. Consolidated Performance Summary

Table IV consolidates key quantitative results across all three simulation domains.

VII. CONCLUSION AND FUTURE SCOPE

A. Conclusion

This paper presents and assesses an integrated FBG-based SHM system for vibration monitoring of underground pipeline infrastructure, which integrates COMSOL Multiphysics, OptiSystem and MATLAB within a physically consistent analytical framework. The framework's performance is validated by key results: strain sensitivity 1.0-1.2pm/$\mu\varepsilon$, temperature

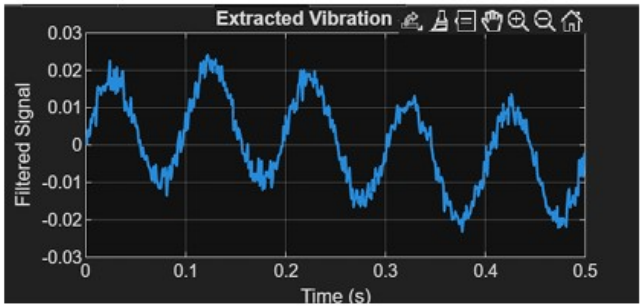


Fig. 25. Extracted vibration signal after high-pass filtering showing oscillations with amplitude ±0.025nm corresponding to pipeline vibration-induced dynamic strain.

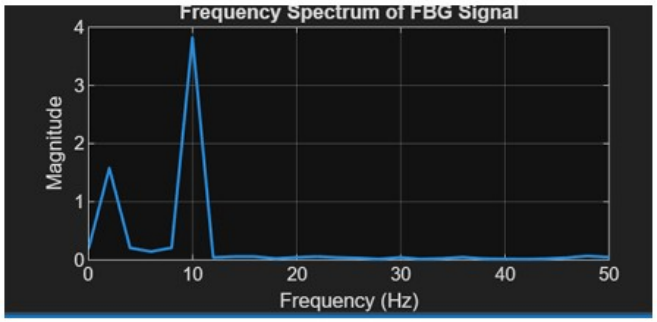


Fig. 26. FFT magnitude spectrum of the processed FBG signal showing a strong vibration peak at ≈10 Hz. The sharp peak indicates successful thermal drift and noise.

TABLE IV CONSOLIDATED SIMULATION RESULTS SUMMARY

Parameter	Value	Significance
Strain sensitivity	1.0–1.2pm/$\mu\varepsilon$	Detects μ-scale deformation
Temp. sensitivity	14.3pm/°C	Enables thermal compensation
Optimal L (grating)	10–15mm	Max. reflectivity & SNR
Peak reflectivity	69% @ 15mm	Strong Bragg reflection

©IJRASET: All Rights are Reserved

Bandwidth (FWHM)	35pm @ 15mm	High wavelength resolution
SNR (optical)	98.4dB	Excellent signal quality
Temp. SNR	91dB	Minimal thermal noise
Linearity (R^2)	0.99	Linear temp. response
Detected frequency	≈10Hz	Traffic-induced vibration
Eff. mode index	1.5	Validates optical model
Peak COMSOL stress	>800MPa	Critical failure zone

sensitivity 14.3pm/°C with R^2 = 0.99, optimal grating length 10-15mm for 69% reflectivity and 98.4dB SNR, and dominant vibration frequency detection at 9.98Hz. The COMSOL stress-corrosion model shows that material degradation results in increasing local stress, measurable by FBG sensors. The MATLAB-based signal processing module effectively extracts vibration frequency from signals with thermal drift and noise. The immunity to EMI, distributed sensing ability and longterm stability of the proposed system confirms the potential of FBG-based technology in next-generation underground infrastructure monitoring.

B. Future Scope

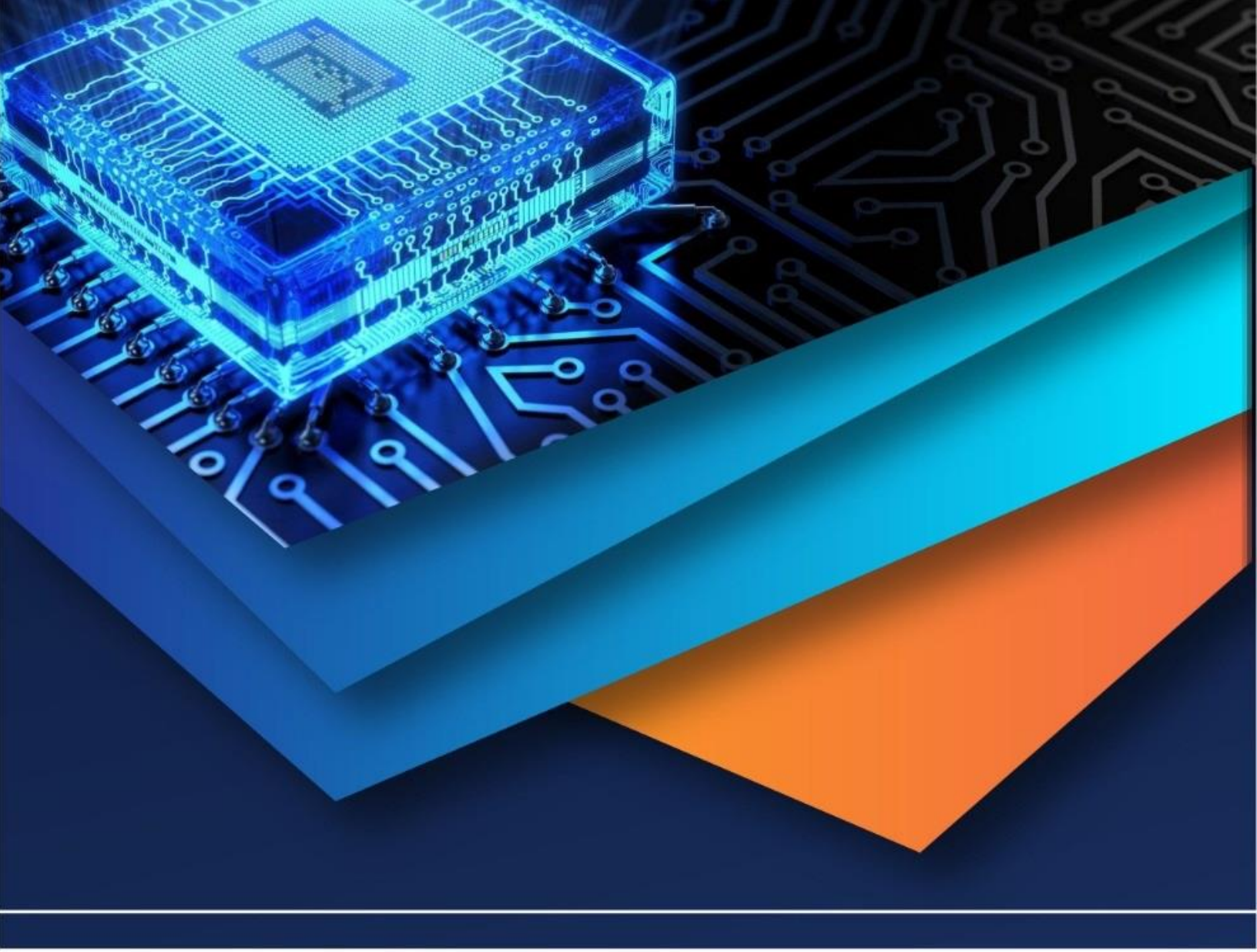
The next steps in this research are: (i) chirped, apodized, or phase shifted FBG designs for increased selectivity; (ii) machine learning for automatic anomaly classification with continuous FBG data; (iii) IoT wireless data monitoring for centralised real-time pipeline operation monitoring; (iv) physical modelling and underground field testing; (v) multi-parameter sensing (strain, temperature, pressure, acoustic) with the FBG; and (vi) adaptation to bridges, dams and railways.

Novelty Statement: The key contribution of this study lies in the first simultaneous use of three different simulation software (COMSOL Multiphysics, OptiSystem, and MATLAB) in one physically continuous framework for the vibration monitoring of underground pipelines. Rather than focusing on structural analysis, optical simulation, or signal processing as discrete tasks as was done in previous papers, this work provides a quantitative physical link from COMSOL-calculated von Mises stress, to Hooke's Law strain, to OptiSystem-simulated Bragg wavelength shift, to MATLAB FFT vibration frequency. The comprehensive grating length study offering practical design insight (optimal: 10-15mm), and the successful temperature compensation technique to pinpoint a 10Hz vibration signature from a composite signal are novel contributions to the FBG-based SHM techniques.

REFERENCES

[1] C. V. N. Bhaskar, S. Pal, and P. K. Pattnaik, "Recent advancements in fiber Bragg gratings based temperature and strain measurement," Results in Optics, vol. 5, p. 100130, 2021.
[2] A. Tripathy, "Evaluation of an optical fiber Bragg grating as a strain sensor," in Proc. VSPICE Conf., 2020.
[3] A. S. More, P. S. Lad, S. R. Krishnan, and S. R. Bhosale, "Performance analysis of strain sensor based on fiber Bragg grating," ITM Web of Conferences, vol. 32, p. 03010, 2020.
[4] X. Qiao, Z. Shao, W. Bao, and Q. Rong, "Fiber Bragg grating sensors for the oil industry," Sensors, vol. 17, no. 3, p. 429, 2017.
[5] M. I. M. Razi, M. R. C. Beson, S. N. Azemi, and S. A. Aljunid, "FBG sensor strain performance analysis using OptiSystem software tools," Indonesian J. Elect. Eng. Comput. Sci., vol. 14, no. 2, pp. 564–572, 2019.
[6] IANS, "Gas leak from ONGC pipeline in Andhra's Kakinada," The Economic Times Energy World, Aug. 2025.
[7] "Industrial pipeline risk reports," Global Times, 2019. [Online]. Available: https://www.globaltimes.cn/content/827035.shtml
[8] W. Chalgham, K.-Y. Wu, and A. Mosleh, "External corrosion modeling for an underground natural gas pipeline using COMSOL Multiphysics," in Proc. COMSOL Conf., Boston, 2019.
[9] A. D. Kersey et al., "Fiber grating sensors," J. Lightw. Technol., vol. 15, no. 8, pp. 1442–1463, 1997.
[10] R. Kashyap, Fiber Bragg Gratings, 2nd ed. Academic Press, 2010.
[11] B. Lee, "Review of the present status of optical fiber sensors," Opt. Fiber Technol., vol. 9, no. 2, pp. 57–79, 2003.
[12] Technica Optical Components, "T99 High Strength FBG Sensor Datasheet," Atlanta, GA, USA, 2023.

©IJRASET: All Rights are Reserved



10.22214/IJRASET

45.98

IMPACT FACTOR: 7.129

IMPACT FACTOR: 7.429

INTERNATIONAL JOURNAL FOR RESEARCH

IN APPLIED SCIENCE & ENGINEERING TECHNOLOGY

Call : 08813907089 (24*7 Support on Whatsapp)